

# Computer Methods in Biomechanics and Biomedical Engineering

ISSN: (Print) (Online) Journal homepage: <https://www.tandfonline.com/loi/gcmb20>

## An analysis of the relationship between microneedle spacing, needle force and skin strain during the indentation phase prior to skin penetration

Matthew R. Potts, Sam L. Evans, Rhys Pullin, Sion A. Coulman, James C. Birchall & Hayley Wyatt

To cite this article: Matthew R. Potts, Sam L. Evans, Rhys Pullin, Sion A. Coulman, James C. Birchall & Hayley Wyatt (2022): An analysis of the relationship between microneedle spacing, needle force and skin strain during the indentation phase prior to skin penetration, Computer Methods in Biomechanics and Biomedical Engineering, DOI: [10.1080/10255842.2022.2136486](https://doi.org/10.1080/10255842.2022.2136486)

To link to this article: <https://doi.org/10.1080/10255842.2022.2136486>



© 2022 The Author(s). Published by Informa UK Limited, trading as Taylor & Francis Group.



Published online: 24 Nov 2022.



[Submit your article to this journal](#)



Article views: 47



[View related articles](#)



[View Crossmark data](#)

# An analysis of the relationship between microneedle spacing, needle force and skin strain during the indentation phase prior to skin penetration

Matthew R. Potts<sup>a</sup> , Sam L. Evans<sup>a</sup> , Rhys Pullin<sup>a</sup> , Sion A. Coulman<sup>b</sup> , James C. Birchall<sup>b</sup>  and Hayley Wyatt<sup>a</sup> 

<sup>a</sup>School of Engineering, Cardiff University, Cardiff, UK; <sup>b</sup>School of Pharmacy and Pharmaceutical Sciences, Cardiff University, Cardiff, UK

## ABSTRACT

Microneedle (MN) array patches present a promising new approach for the minimally invasive delivery of therapeutics and vaccines. However, ensuring reproducible insertion of MNs into the skin is challenging. The spacing and arrangement of MNs in an array are critical determinants of skin penetration and the mechanical integrity of the MNs. In this work, the finite element method was used to model the effect of MN spacing on needle reaction force and skin strain during the indentation phase prior to skin penetration. Spacings smaller than 2–3 mm (depending on variables, e.g., skin stretch) were found to significantly increase these parameters.

## ARTICLE HISTORY

Received 11 January 2022  
Accepted 11 October 2022

## KEYWORDS

Microneedles; microneedle spacing; skin penetration; finite element analysis

## 1. Introduction

Microneedle (MN) array patches provide a new approach to the transdermal delivery of therapeutics. Unlike traditional millimeter dimension needles and syringes, which are typically inserted into the subcutaneous region, muscle or vasculature, MNs are designed to deliver drugs or vaccines into the superficial skin tissue (i.e., the epidermis or dermis; Prausnitz 2004). MNs are typically just a few hundred microns at their widest point and less than 1 mm in length, such that, when pushed into the skin, they come to rest in the epidermis or dermis, which lies approximately 0.02–1 mm beneath the skin surface (Guillot et al. 2020).

To deliver sufficient doses, MNs are often arranged into arrays, typically consisting of 100–1000 MNs, which are administered simultaneously. One challenge, however, is achieving repeatable and consistent skin penetration with all MNs on a single array. This reproducibility is a key aspect of performance for both patient safety and efficacy. A key design aspect is the spacing between the needles (often termed MN density). Few studies have investigated the relationship between MN spacing and the determinants of penetration and the results are inconsistent, especially with respect to penetration force (PF - the reaction force preceding the characteristic drop following skin

puncture). Kochhar et al. (2013) found that increasing the spacing between MNs (between 0.4 and 2.4 mm) increased needle penetration efficiency (PE – percentage of needles on an array successfully penetrating the skin) in rodent skin, with the increase varying from 2 to 52% of needles for different needle and array designs. There was a consistent increase in PF with increased spacing. However, Olatunji et al. (2013) measured a decrease in PF with increasing needle spacing in porcine skin. They decreased the number of needles in the array (from 16 to 4) as the spacing increased (from 0.33 to 0.90 mm), possibly explaining the reduction in force. Olatunji et al. supported their experimental observations with data from a Finite Element Model (FEM) of two MNs inserting into skin, with similar results, but did not provide information on PE. A third investigation by Shu et al. (2021) found a decrease in PF with increased spacing (0.156–1.75 mm range studied), but also an increase in PE, while Oh et al. (2008) observed an increasing proportion of successful puncture holes when increasing MN spacing. Donnelly et al. (2010) found that spacing had no effect on depth of penetration when applying needles of the same height at the same force (MN base interspacing range of 0.03–0.6 mm studied), while experiments by Verbaan et al. (2008) suggested that smaller MN spacings may lead to reduced depth of penetration.

CONTACT Matthew R. Potts  [pottsm@cardiff.ac.uk](mailto:pottsm@cardiff.ac.uk)

© 2022 The Author(s). Published by Informa UK Limited, trading as Taylor & Francis Group.

This is an Open Access article distributed under the terms of the Creative Commons Attribution License (<http://creativecommons.org/licenses/by/4.0/>), which permits unrestricted use, distribution, and reproduction in any medium, provided the original work is properly cited.

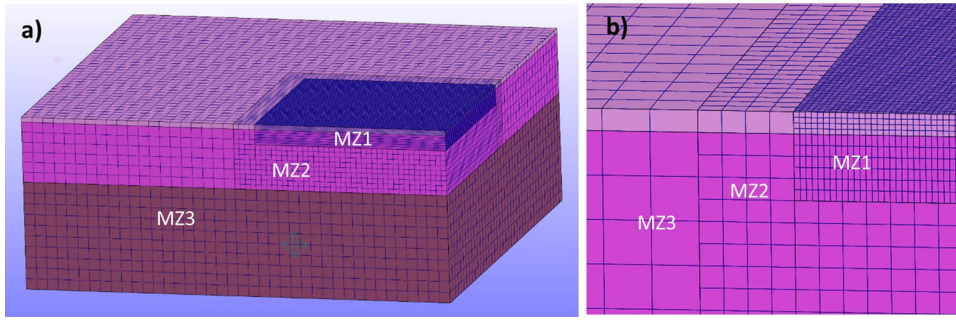


**Figure 1.** Layout of the skin block. Shown in (a) is the entire quartered skin block with mesh zones labelled. Shown in (b) is a zoom-in of the block, showing the relationship between the three mesh zones. In this diagram, MZ1 is of the level 4 refinement.

Although there appears to be an emerging consensus on the relationship between MN spacing and PE, the relationship between spacing and PF remains much less clear. This may be due to the difficulty of obtaining individual force measurements for each MN on an array. Furthermore, of the six studies mentioned above, only Shu et al. (2021) provide substantial information on the relationship between spacing and skin strain (Olatunji et al. only provided qualitative contour plots of the strain distribution). Shu et al. found that the predicted skin strain increased with decreasing MN spacing.

Skin is a complex structure that varies significantly in both structure and mechanical properties depending on the species, the individual and the specific site. To date, there has been no comprehensive investigation into the effect of these variations on the relationship between MN spacing and penetration, which may contribute to the contradictory findings seen in the literature. The aim of this study was to investigate this. FEM was used to model the first phase of MN insertion: skin indentation. A two-needle indentation model was used to establish the relationship between MN spacing, needle reaction force (RF) and skin strain with an initial parameter set, and then a sensitivity analysis was used to investigate the effect of skin property/needle geometry variation. A nine-needle simulation was used to investigate whether the findings hold true for a larger array.

## 2. Methods

The quasi-static finite element analysis was carried out using FEBio (Maas et al. 2012). A one-term, nearly incompressible, hyperelastic Ogden material model was used to model each skin layer using material constants measured by Groves et al. (2012) (see Section 2.4.1 for further details). The strain energy function is presented in Equation (1), where  $\mu$

and  $\alpha$  are material constants that correspond to the  $\mu$  and  $\alpha$  constants measured by Groves et al.,  $\tilde{\lambda}$  are the deviatoric principal stretches,  $U(J)$  is the volumetric component and  $J$  is the determinant of the deformation gradient.

$$W(\lambda_1, \lambda_2, \lambda_3, J) = \frac{\mu}{\alpha^2} \left( \tilde{\lambda}_1^\alpha + \tilde{\lambda}_2^\alpha + \tilde{\lambda}_3^\alpha - 3 \right) + U(J) \quad (1)$$

### 2.1. Two-needle model

#### 2.1.1. Skin geometry and mesh

The skin was represented by a  $6 \times 6$  mm block, comprising three layers corresponding to the epidermis, dermis and hypodermis. The thickness of the block varied as part of the sensitivity analysis (Section 2.1.3). Symmetry boundary conditions were used such that the model represented a larger  $12 \times 12$  mm block.

The skin block consisted of three regions of HEX8 elements with varying mesh densities (Figure 1). The region labelled MZ1 in Figure 1 ( $2.7 \times 2.7 \times 0.28$  mm) was the densest region and represented the area where the needles contact the skin. The other two regions (MZ2 and MZ3) had a coarser mesh. The different regions were connected using facet-to-facet tied contacts.

To determine the optimal density of the MZ1 mesh region, a convergence analysis was performed. The mesh was varied as detailed in Table 1, with the mesh density of the other regions remaining constant ( $\sim 2540$  and  $\sim 317$  per  $\text{mm}^3$ , respectively). For the convergence study, the thickness of the epidermis, dermis and hypodermis were set to 0.07 mm (Gambichler et al. 2006), 0.84 mm (Moore et al. 2003) and 1.5 mm (Groves et al. 2012), respectively (Table 2). Needle RF versus needle spacing and 1st principle Lagrangian skin strain versus needle spacing curves were extracted to determine the optimal mesh. Unlike needle PF, needle RF refers to the force going through

**Table 1.** Element dimensions/counts present in the four different refinement models of the mesh sensitivity analysis. Element dimensions are presented as horizontal length ( $x=y$ ) versus height ( $z$ ).

Refinement model	Epidermis MZ1		Dermis MZ1	
	Element dimensions (mm)	Element number	Element dimensions (mm)	Element number
Level 1 (L1)	$0.075 \times 0.07$	1296	$0.075 \times 0.07$	3888
Level 2 (L2)	$0.0375 \times 0.035$	10368	$0.0375 \times 0.035$	31104
Level 3 (L3)	$0.025 \times 0.0233$	34992	$0.025 \times 0.035$	69984
Level 4 (L4)	$0.01875 \times 0.0175$	82944	$0.01875 \times 0.035$	124416

See Table 2 for further information on the control model feature set used in the mesh sensitivity analysis.

**Table 2.** Skin layer thicknesses and Ogden material properties of the initial control model.

Skin layer	Layer thickness (mm)	Ogden material parameters		
		$\mu$ (MPa)	$\alpha$	K (MPa)
Epidermis	0.07	4.1	2.98	4100
Dermis	0.84	0.0266	3.29	22.6
Hypodermis	1.5	0.0104	13.6	10.4

This is in combination with rounded needle tip and no pre-stretch. See section 2.1.1 and section 2.1.4 for the context of the features/values implemented and the relevant references.

the needle for a given displacement and so varies throughout needle advancement.

### 2.1.2. Needle geometry

The needle tip shape was varied to understand the effect of needle tip geometry on MN spacing, needle RF and skin strain. A blunt tip, rounded tip and pointed tip were investigated (Figure 2). The rounded tip was used in models unless otherwise stated. The tip diameters of the blunt, rounded and pointed geometries were approximately 75, 30 and 5  $\mu\text{m}$ , respectively. All tips had a base diameter of 110  $\mu\text{m}$ .

All tips were formed from a body region (in yellow, Figure 2) and a cap region (in green). The body was modelled as stainless steel (linear elastic,  $E=2 \times 10^8 \text{ MPa}$ ,  $\nu=0.3$ ). The rounded and pointed tips were meshed with TET4 elements, while the blunt tip was meshed with HEX8 elements. The cap region was modelled as a rigid body and formed from either extruded PENTA6 or HEX8 elements. Facet-to-facet sliding contacts were used between the skin and the needle tip.

### 2.2.3. Boundary conditions

The symmetry planes and boundary edges of the skin block were prevented from displacing perpendicular to their surfaces. The bottom of the block was constrained in the vertical direction.

A single half-needle tip was displaced in a downward direction onto one of the cut edges of the quartered skin block (Figure 3). The spacing of the two simulated needles was controlled by varying the position of the half needle. The needle was displaced vertically downwards by a prescribed displacement of 0.3 mm.

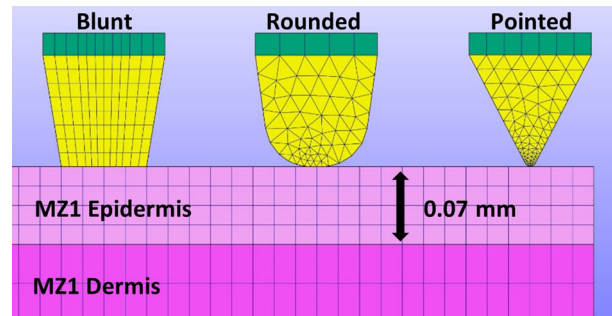


**Figure 2.** Microneedle tip geometries used in the two and nine needle spacing analyses, resting on the skin block. Shown in the middle is the rounded needle tip geometry, whilst shown on the left and right are the blunt and pointed needle tips, respectively. The yellow and green portions represent the body and cap regions, respectively. Skin mesh is of the L4 mesh refinement (see Figure 1) and is the mesh used throughout the two and nine needle spacing analyses.

### 2.1.4. Spacing sensitivity analysis

An initial control model (model 1) was established, with material properties detailed in Table 2, the rounded tip and no pre-stretch. Each layer was modelled using an Ogden material model (see start of methods section), using the average  $\mu$  and  $\alpha$  constants reported by Groves et al. (2012).

Seventeen additional variations of the model were then run. In models 2–7 the mechanical properties of the skin were varied (using the maximum and minimum  $\mu$  and  $\alpha$  constants measured by Groves et al. 2012), in models 8–14 the thickness of the skin layers was varied (halved, doubled and quadrupled), and in models 15–16 the effect of skin pre-stretch was explored (using 10 and 20% biaxial pre-stretch; Evans and Holt 2009 and Flynn et al. 2011 measured pre-stretch of approximately 20%). In models 17–18 the geometry of the needle was varied. The differences are summarised in Table 3; all other parameters remained the same as the control model. For each variation, nine different needle spacings were investigated, from 0.5 to 4.5 mm at 0.5 mm intervals. The maximum was chosen following a pilot study to identify when values stopped changing with increasing needle spacing. However, this is much larger than the 2.4 mm maximum spacing studied by Kochhar et al.

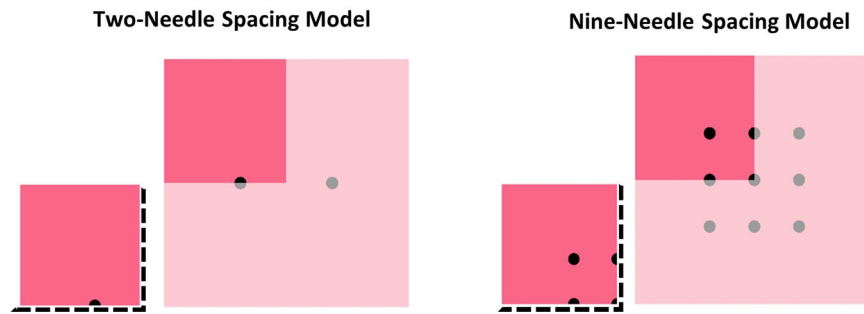


**Figure 3.** Top-down views of the modelling format used to perform the two- and nine-needle spacing analyses. Shown in solid colours are the geometries present in the models. Shown in transparent colours are the geometries modelled as a result of the symmetry constraints on the solid colour geometries. Needle = black; skin block = pink. Cut-edges are indicated by dashed black border; all other edges represent boundary-edges. Geometries and spacings are not shown true to size within this schematic for clarity.

**Table 3.** Features and values used in the 18 versions of the two-needle spacing analysis.

Version	Feature	Value(s)
1	Control parameter set	–
2	Minimum epidermis Ogden values	$\kappa = 1210 \text{ MPa}$ , $\mu = 1.21 \text{ MPa}$ , $\alpha = 1.65$
3	Maximum epidermis Ogden values	$\kappa = 7480 \text{ MPa}$ , $\mu = 7.48 \text{ MPa}$ , $\alpha = 6.35$
4	Minimum dermis Ogden values	$\kappa = 10.52 \text{ MPa}$ , $\mu = 0.0152 \text{ MPa}$ , $\alpha = 2.70$
5	Maximum dermis Ogden values	$\kappa = 30.9 \text{ MPa}$ , $\mu = 0.0309 \text{ MPa}$ , $\alpha = 4.41$
6	Minimum hypodermis Ogden values	$\kappa = 8.5 \text{ MPa}$ , $\mu = 0.0085 \text{ MPa}$ , $\alpha = 3.43$
7	Maximum hypodermis Ogden values	$\kappa = 13.2 \text{ MPa}$ , $\mu = 0.0132 \text{ MPa}$ , $\alpha = 29.8$
8	Halved epidermis thickness	$h = 0.0375 \text{ mm}$
9	Doubled epidermis thickness	$h = 1.4 \text{ mm}$
10	Halved dermis thickness	$h = 0.42 \text{ mm}$
11	Doubled dermis thickness	$h = 1.68 \text{ mm}$
12	Halved hypodermis thickness	$h = 0.75 \text{ mm}$
13	Doubled hypodermis thickness	$h = 3 \text{ mm}$
14	Quadrupled hypodermis thickness	$h = 6 \text{ mm}$
15	10% skin stretch	$\lambda = 10\%$
16	20% skin stretch	$\lambda = 20\%$
17	Blunt needle tip	–
18	Pointed needle tip	–

See section 2.1.1 and section 2.1.4 for the context of the features/values implemented and the relevant references.

(2013), one of the largest spacings seen in a fabricated MN array (to the authors' knowledge). The minimum spacing of 0.5 mm was chosen as a typical low spacing seen in fabricated MN arrays (Donnelly et al. 2010; Kochhar et al. 2013; Olatunji et al. 2013; Larraneta et al. 2016; Shu et al. 2021).

#### 2.1.4. Pre-stretch model variation

To simulate skin pre-stretch, the boundary surfaces were moved parallel to the skin surface (Table 3) and then constrained. To keep the final dimensions of the skin block constant, a scaling transformation (shrinking the block in-plane, whilst stretching it out-of-plane) was applied to the mesh prior to the application of the in-plane stretch. Due to problems encountered with the tied contact between the MZ2 and MZ3 regions when stretched, the MZ2 and MZ3 regions were instead replaced with a continuous region of MZ2 mesh density for these models.

## 2.2. Nine-needle model

The nine-needle models used the same parameters as the two-needle control model. A total of eight models were run, with needle spacings from 0.5 to 2.25 mm, at 0.25 mm intervals. This smaller range was necessitated by the inclusion of a center needle, but still captures the larger spacings typically seen in fabricated MN arrays.

For each model, four needle tips were displaced vertically downwards by 0.3 mm, indenting the skin. Due to symmetry, the model consisted of two half-needles on each cut edge, one quartered-needle on the central corner and one full needle on the interior of the block (Figure 3).

## 2.3. Data processing

For each model, two sets of data were extracted, the RF through the needles and the maximum 1st principal Lagrangian skin strain. For all but the pre-stretch



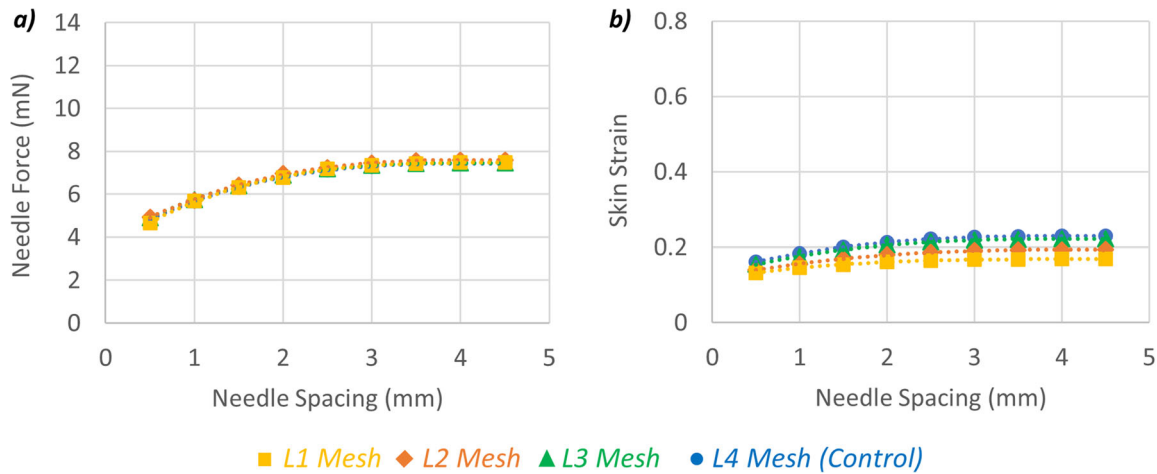


**Figure 4.** Effect of MZ1 element density on needle reaction force (a) and skin strain (b). Force values represent force through each needle, which are identical due to assumed symmetry. The 3.5, 4.0 and 4.5 mm needle spacing data points of the L3 Mesh data series represent extrapolated values.

models, the skin strain from indentation was simply taken as the absolute value outputted by the model. For the pre-stretch models, the skin strain from indentation was calculated by subtracting the strain value measured at the end of the bi-axial stretch step from the value measured during indentation. A target needle displacement of 0.3 mm was initially attempted; however, this proved difficult to achieve for some of the models (e.g., double-thickness epidermis). Since all but two models exceeded 0.25 mm needle displacement, 0.25 mm was chosen as the displacement that data was extracted at. Given that Römgens et al. (2014) measured an average displacement-at-puncture of just under 1 mm for their 5  $\mu$ m diameter tip microneedle inserting into skin at quasi-static insertion velocity (0.05 mm/s), it is assumed that all three tip types of the present analysis will not have punctured at 0.25 mm displacement.

For the models that exceeded 0.25 mm displacement, a polynomial curve was fitted to the RF/skin strain-displacement data generated from the models and used to interpolate the force and strain at 0.25 mm displacement. These were then plotted against needle spacing. For the model variants which did not exceed 0.25 mm displacement, the equation of the fitted polynomial was used to estimate the probable force and strain at 0.25 mm displacement. The model variants which required extrapolation were the double thickness epidermis models at 2.5, 3.0 and 3.5 mm needle spacing (0.24, 0.22 and 0.23 mm needle displacement reached, respectively) and the L3 mesh models at 3.5, 4.0 and 4.5 mm needle spacing (0.24, 0.24 and 0.24 mm needle displacement reached, respectively).

For each model of the nine-needle spacing analysis, three points were plotted: one for the centre needle

(the single quarter needle), one for the edge needles (average of the two half needles) and one for the corner needle.

### 3. Results

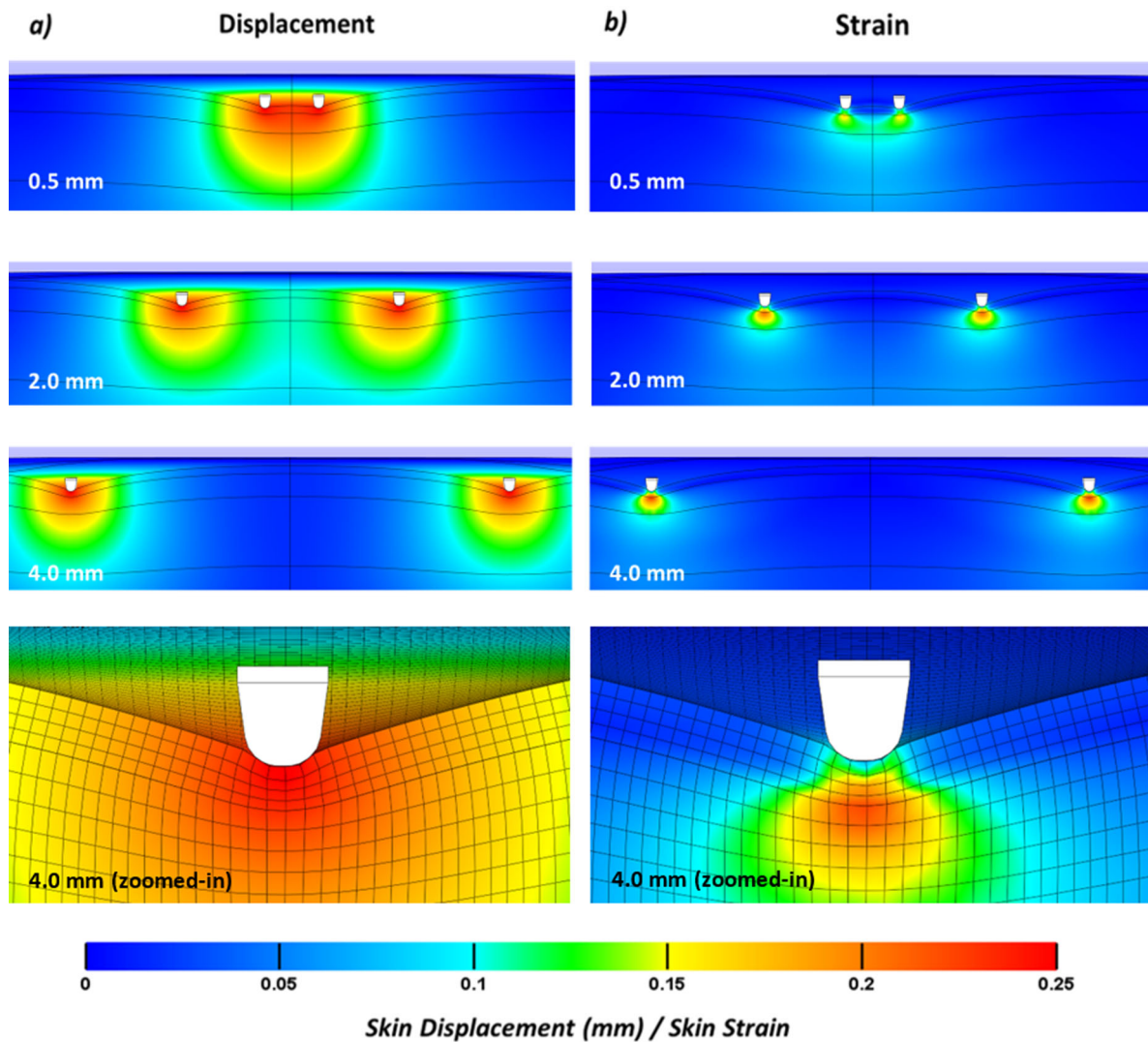
#### 3.1. Mesh sensitivity analysis

Figure 4 shows the results for the mesh sensitivity analysis. Figure 4a demonstrates that needle RF (rounded tip, values represent force through each needle) was independent of the mesh density; however, Figure 4b shows an increase in skin strain for mesh density L1 to L3. A negligible difference in strain was found between L3 and L4 meshes, meaning either mesh would be suitable for this analysis. Mesh L4 was chosen as the final mesh used for both the two-needle spacing analysis and the nine-needle analysis.

It is arguable that the mesh sizes considered in the sensitivity analysis are not sufficient to accurately capture the precise strains directly under the needle tip (especially for the conical tip); however, the L4 mesh was considered to be sufficiently fine for the purposes of capturing general trends.

#### 3.2. Two-needle spacing analysis

Figure 5 shows the skin deformation (displacement and strain at 0.25 mm needle displacement) produced at 0.5, 2.0 and 4.0 mm needle spacing for the control model (Table 3). The skin deformation zones are separated (within the scale scheme used) at 4.0 mm needle spacing, while at 0.5 mm needle spacing, the deformation zones have coalesced. At 2.0 mm, overlapping deformation zones can be seen. The extracted



**Figure 5.** Skin displacement (a) and 1st principal Lagrangian strain (b) at 0.5, 2.0 and 4.0 mm needle spacing (labelled), at needle displacement of 0.25 mm. Needle tips are shown in white. A zoomed-in view is also presented for the 4.0 mm needle spacing model with the mesh visible. The skin strain shown is the absolute value outputted by model (as opposed to the calculated value described in Section 2.3 for the pre-stretch models).

needle RF and skin strain for the control model are shown in Figure 6.

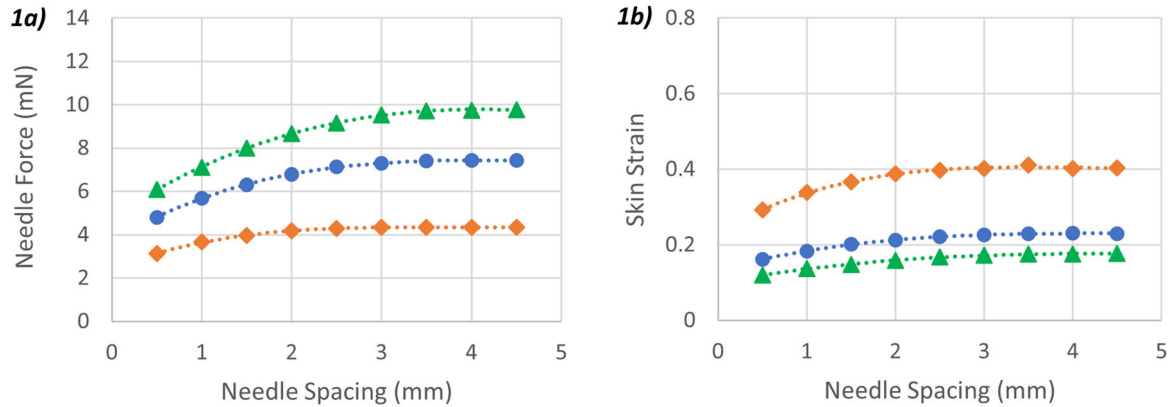
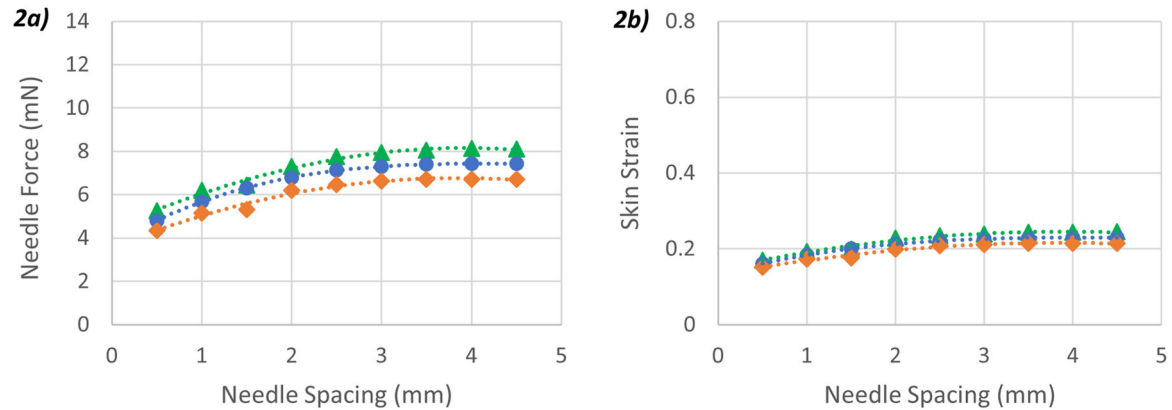
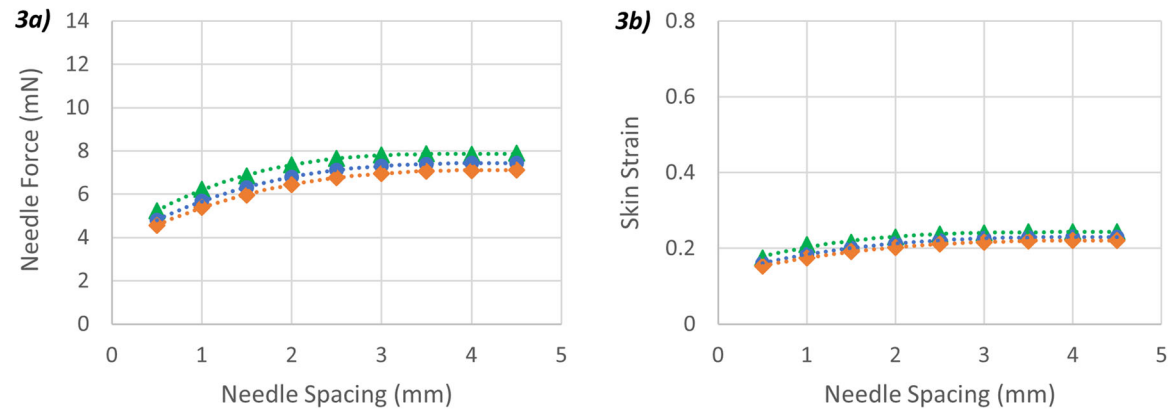
All variations of the two-needle spacing analysis showed a similar relationship with both needle RF and skin strain increasing with needle spacing (Figures 6–9). The exact magnitude of force and strain, however, was found to vary significantly. This led to subtle differences in the shape of the force–spacing curve for each model.

The effect of varying the skin material properties is shown in Figure 6. The material properties of the epidermis had the greatest effect on both the needle RF and the skin strain. When varying the properties of the epidermis within the reported physiological range, the RF increased by an average of 112%, but it only increased by 20 and 13% from the minimum to the maximum stiffness of the dermis and hypodermis.

The relationship between skin stiffness and skin strain was the inverse. The strain at maximum epidermal stiffness, for example, was approximately half that of the strain at minimum stiffness.

The skin layer thickness had a comparable influence (Figure 7); halving the epidermal thickness reduced the RF by 29%, whilst doubling the thickness increased RF by 66%. In contrast, varying the thickness of the hypodermis and dermis had minimal effect, with the thickness of the dermis being the least influential variable investigated within this study. The relationship between skin layer thickness and skin strain was again the inverse.

A small effect on both needle RF and skin strain was measured when varying the hypodermis thickness. The largest effect was found in halving the thickness from 1.5 to 0.75 mm; a negligible difference was found between 3.0 and 6.0 mm.

**Effect of Epidermis Ogden Parameter Variation****Effect of Dermis Ogden Parameter Variation****Effect of Hypodermis Ogden Parameter Variation**

● Control Values (Average) ◆ Minimum Values ▲ Maximum Values

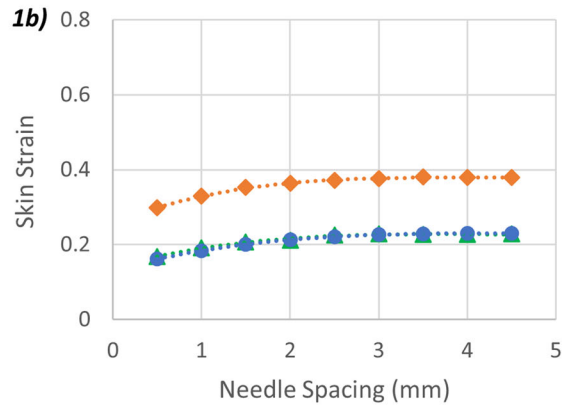
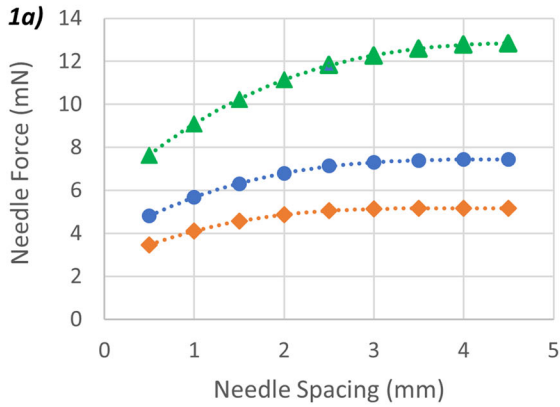
**Figure 6.** Effect of skin layer Ogden parameters on the relationship between needle reaction force and needle spacing (1a–3a) and skin strain and needle spacing (1b–3b). Control values represent the average values measured by Groves et al. (2012). Force values represent force through each needle, which are identical due to assumed symmetry.

The pre-stretch of the skin had the largest effect on the magnitude of the RF (Figure 8), with increases of approximately 195 and 376% between the control versions (no stretch) and the 10 and 20% stretch versions, respectively. A slightly smaller increase was observed in the strain (86 and 192%).

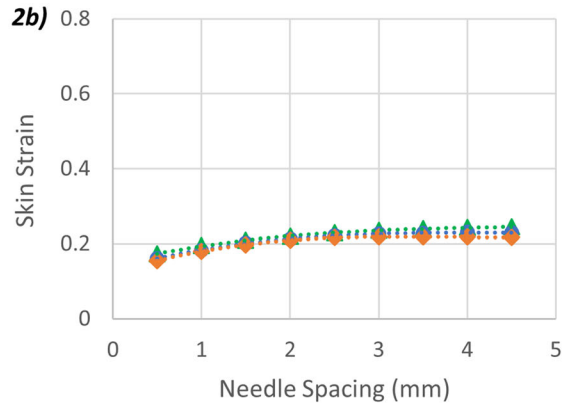
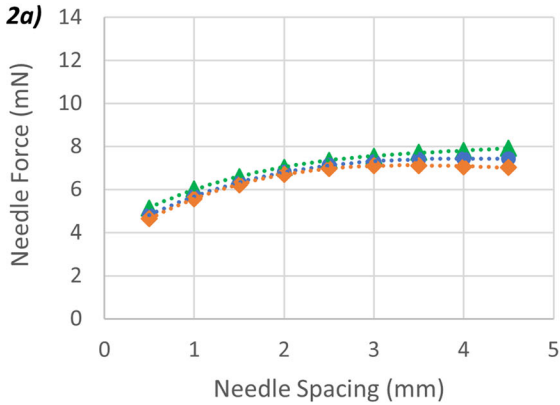
Needle geometry had little effect on either the magnitude of RF or the relationship between RF and needle spacing (Figure 9). The blunt tip increased the RF by approximately 8% compared to the rounded tip, while the pointed tip decreased it by approximately 10%. The pointed tip had the greatest effect



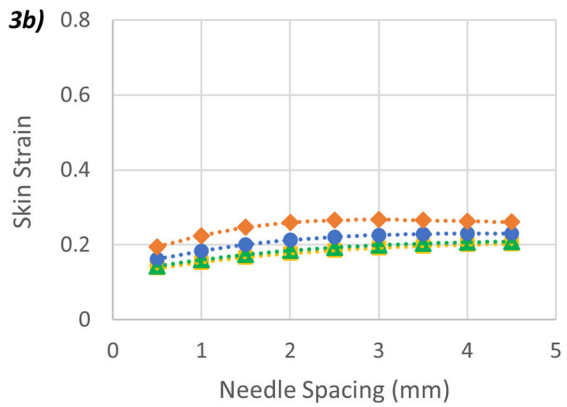
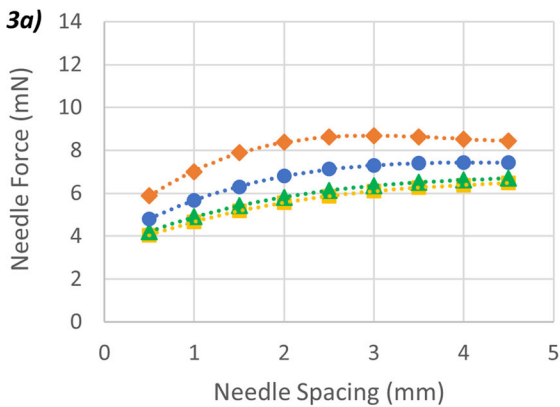
**Effect of Epidermis Thickness Variation**



**Effect of Dermis Thickness Variation**



**Effect of Hypodermis Thickness Variation**



● Control Thickness    ◆ Halved Thickness    ▲ Doubled Thickness    ■ Quadrupled Thickness

**Figure 7.** Effect of skin layer thicknesses on the relationship between needle reaction force and needle spacing (1a–3a) and skin strain and needle spacing (1b–3b). The 2.5, 3.0 and 3.5 mm needle spacing data points of the double thickness epidermis data series represent extrapolated values.

on skin strain, with a 122% increase. A considerably smaller decrease in strain (approximately 10%) was found for the blunt tip.

Presented in Figure 10 are averaged, normalized RF/skin strain–spacing curves for all the variations. This shows that the way in which needle RF and skin

strain increase with needle spacing is only slightly sensitive to major parameter variations (at least of those studied here), possibly indicating that microneedles (in general) have a relatively fixed radius of influence. Both curves reach a plateau at approximately 3.0 mm.

### Effect of Skin Pre-Stretch Variation

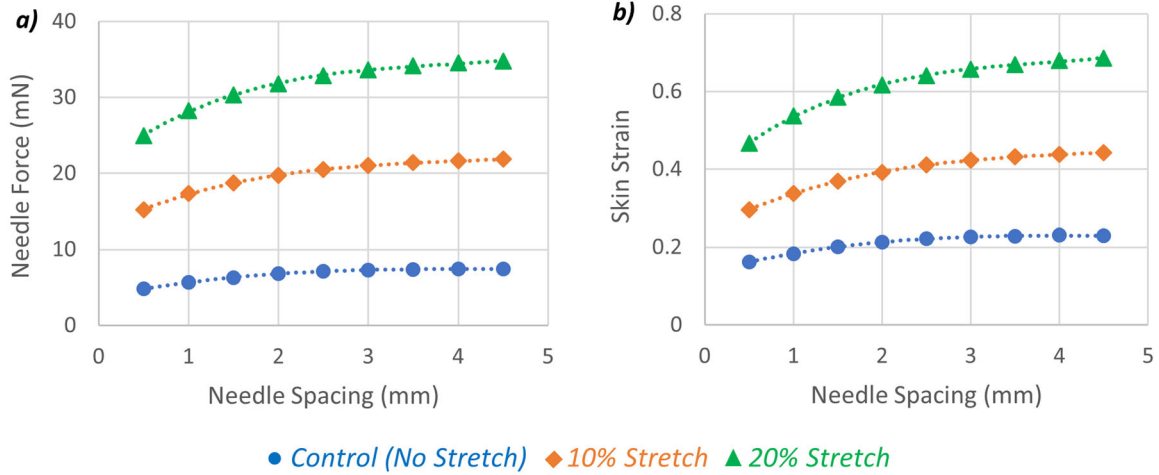


**Figure 8.** Effect of skin pre-stretch on the relationship between needle reaction force and needle spacing (a) and skin strain and needle spacing (b). The skin strain shown is the additional strain due to needle indentation (as defined in Section 2.3).

### Effect of Needle Geometry Variation

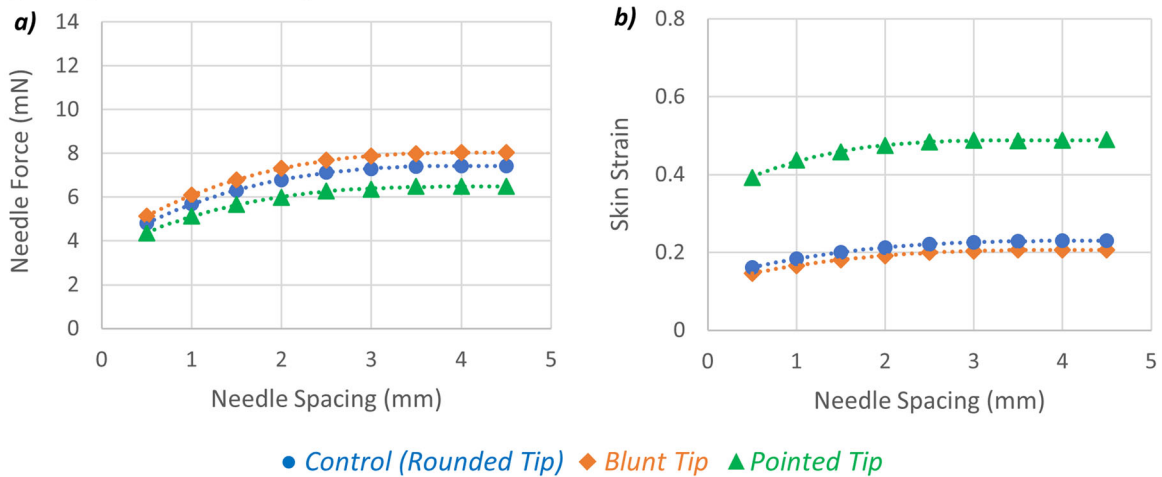


**Figure 9.** Effect of needle geometry on the relationship between needle reaction force and needle spacing (a) and skin strain and needle spacing (b).

### 3.3. Nine-needle spacing analysis

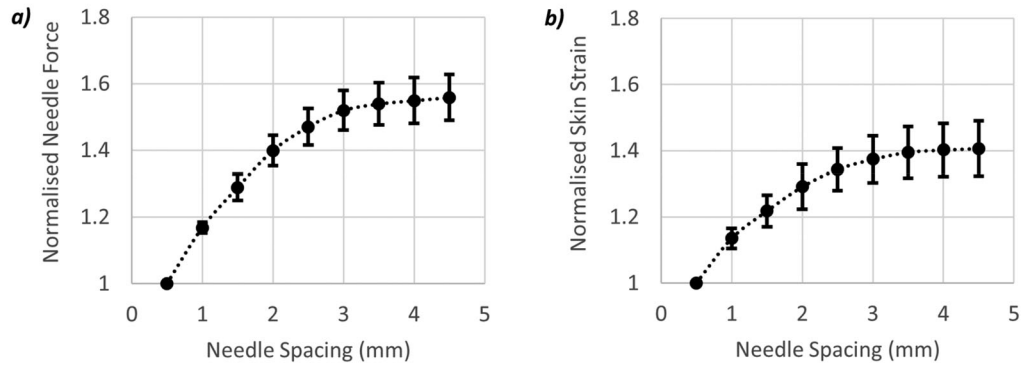
The nine-needle spacing analysis produced three RF/skin strain-spacing curves for the center needle, edge needles and corner needles (Figure 11). The corner needles experienced the highest RF, the centre needle experienced the lowest RF and the edge needles were approximately halfway between the two. This was echoed in the strains.

For both the needle RF and skin strain measurements, the three curves converge with increasing needle spacing (as one would expect, given that the behaviour of a single microneedle-skin interaction should be achieved for all needles as the spacing increases to infinity). This was especially the case with the RF measurement, where the edge and corner

needles were found to experience 510 and 929% of the center needle's RF at 0.5 mm needle spacing, but only 106 and 112% at 2.25 mm spacing. In contrast, the edge and corner needles experienced 311 and 446% of the center needle's skin strain at 0.5 mm needle spacing, but only 100 and 112% at 2.25 mm spacing.

## 4. Discussion

MN spacing is an important factor when optimising the performance of MN arrays (Kochhar et al. 2013; Olatunji et al. 2013) and the aim of this study was to use FEM to understand the effect of spacing on array performance. Figure 10 demonstrates that increased

**All Variations**

**Figure 10.** Average of all force-spacing (a) and strain-spacing (b) curve variations. Normalised reaction force/skin strain is equal to the reaction force/strain at the spacing divided by the reaction force/strain at 0.5 mm needle spacing. Error bars show standard deviation.

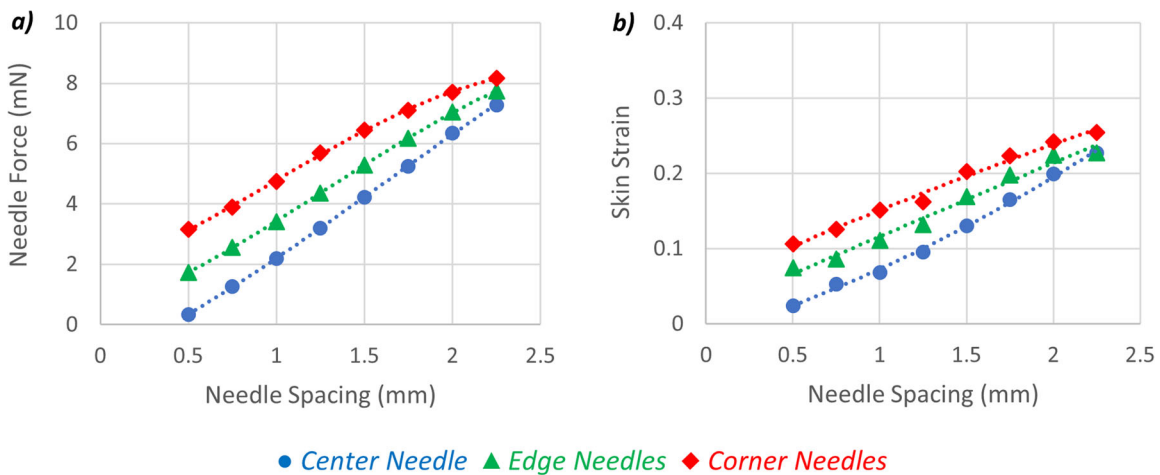


**Figure 11.** Reaction force (a)/skin strain (b)-spacing curves extracted from the nine-needle spacing analysis.

needle spacing results in an increase in both needle RF and skin strain. If a high skin strain is considered as a damage/puncture criterion (many failure strain values have been recorded for skin (Joodaki and Panzer 2018), yet no consensus has been reached as to whether stress or strain is more appropriate) then it would follow that these results are consistent with the emerging consensus that PE increases with spacing. However, in terms of PF, the measured increase in needle RF with spacing appears to be consistent with the findings by Kochhar et al. (2013), which found an increase in PF with spacing, and contrary to the findings by Olatunji et al. (2013) and Shu et al. (2021), which found a decrease. This increase in needle RF with spacing measured in the present work can be explained by there being decreasing overlap of deformation zones under each needle (as displayed in Figure 5), resulting in decreased sharing of the work involved in deforming the skin and, therefore, an increase in the force through each needle. This

increase in needle RF (for a given displacement) with spacing, would then give rise to a higher indentation stiffness with spacing and, therefore, a higher strain with spacing. The increase in PF with spacing can lastly be explained by a decreasing stretch-by-neighbouring-needles effect, wherein at small spacings, the skin under each needle will be stretched by the indentation effect of its neighbouring needles, leading to higher strain for a given force and, therefore, a lower PF at the failure strain. This effect would decrease as the spacing increased and, as a result, one would expect the PF to increase.

The variation in force and strain stabilised (within 5%) at a needle spacing of 2–3 mm (depending on the precise combination of variables), suggesting that the optimal spacing lies approximately within this range. Any needle spacings less than 2 mm will, therefore, be likely to affect any aspects of needle array mechanical performance which are influenced by these factors (such as penetration efficiency/force), with smaller

spacings having a greater influence. Spacings greater than 2 mm, however, are likely to make many arrays impractically large and a balance will need to be sought with respect to other design factors.

When considering array design, it is also essential to consider the natural variation that can occur in skin properties. There is a wide range of skin layer thickness and mechanical properties reported in the literature, and knowing which parameters to select for modelling can be challenging (Groves et al. 2012). This study aimed to understand the impact of these parameters on the optimisation of needle spacing. The results (Figures 6–8) show how the needle RF and skin strain vary when changing these parameters. As can be seen in Figures 6–8, the same trends are apparent in all the data, irrespective of the geometric and mechanical properties (albeit with varying overall force/strain magnitude). This suggests that, while these parameters may affect the overall PE of a particular needle design (due to their effect on general force/strain magnitude under each needle), and therefore the overall force required to insert the array, the optimum needle spacing of the array is somewhat independent of these parameters.

In this study, skin pre-stretch, skin layer thickness and skin layer mechanical properties were all systematically varied. Of these three factors, pre-stretch was found to be the most influential in terms of both effect on magnitude of needle RF and skin strain. Not only was a substantial increase in needle RF found (376% increase with 20% strain), but also in the strain under the needle (192% increase with 20% strain), suggesting that pre-stretch leads to needles puncturing at a lower displacement (due to faster build-up towards failure strain). This is consistent with the limited quantitative data in the literature, which demonstrates increasing PE with pre-stretch (Kim et al. 2018; Sabri et al. 2020; Shu et al. 2021), as earlier puncture should translate to increased PE. The increase in skin strain with stretch measured in the present work can be explained by the fact that the dermis and hypodermis stiffen more with strain than the epidermis (Groves et al. 2012), leading to a narrowing of the difference between the stiffness of the epidermis and dermis. With a greater homogeneity in stiffness, a smaller proportion of the needle displacement is then absorbed through deflection of the stiff epidermis into the less stiff dermis, leading to a greater indentation depth for a given needle displacement and, therefore, a higher strain. In terms of PF and pre-stretch, however, there is again disagreement, as Sabri et al. found increasing PF with pre-stretch,

Shu et al. found a decrease and Kim et al. found no effect. Although an increase in pre-stretch led to an increase in strain in the present study, it also produced a much greater increase in RF, suggesting a higher PF would have been achieved at the failure strain (despite a lower displacement-at-puncture). Overall, however, the results of this study further suggest that application sites, techniques or applicators that keep the skin under tension may be beneficial to MN insertion (due to greater PE). Furthermore, these results further emphasize the importance of including pre-stretch when performing experiments in skin. However, the wide variability in skin pre-stretch between subjects, with age, in different parts of the body and with movement of adjacent joints makes this difficult to quantify. This may account for some of the wide variability in PE found for many micro-needle systems.

When considering the variation in layer thickness and mechanical properties, changes to the epidermis were found to be most influential. A thicker epidermis resulted in a greater needle RF, but a lower skin strain. If the skin strain is considered as a damage/puncture criterion, then this would indicate that with a thicker epidermis, the skin will be more difficult to puncture, and will require a higher PF. These same trends can be seen when increasing the stiffness of the epidermis (an increase in stiffness resulted in a greater needle RF, but a lower skin strain). The variation in epidermis thickness and stiffness could again have significant implications for optimising the geometry of the individual needles, and is an important factor to consider, given the natural variation in epidermis properties that occurs within the population (Gambichler et al. 2006). Except where the hypodermis was made much thinner than it would be in typical administration sites (0.75 mm thickness model), varying the thicknesses and mechanical properties of the other layers was found to have little effect. This suggests that the site of MN administration may not be critical, except where the hypodermis is especially thin (e.g., over bony prominences).

When studying the effect of individual needle geometry, the same trends for optimal needle spacing remained (2–3 mm spacing). Furthermore, at a needle displacement of 0.25 mm, there was little variation in the RF through the needles and so the optimal spacing is likely to be independent of sharpness. The geometry did have a large impact on the general magnitude of strain within the skin, however. Again, if a high skin strain is considered as a damage/puncture criterion, then a sharper needle is likely to puncture

the skin at lower indentation magnitudes and at lower force than a blunter needle, as one would expect (consistent with the findings of Römgens et al. 2014).

Comparing the results from the two-needle and nine-needle models, the same trends could be seen, with the same optimal spacing. This suggests that the modelling of two needles is likely to be sufficient in investigating optimal MN array parameters such as spacing, and that results from this could easily be scaled up to larger arrays. However, the well-documented anisotropy of skin (Groves et al. 2012; Joodaki and Panzer 2018) is likely to have some effect on the needle forces and skin strains measured across the needle-skin interaction sites of three-dimensional arrays, which requires investigation (though the anisotropy is mostly relevant to in-plane stretching of the skin and predominantly due to the fibres deeper in the dermis, making it potentially less relevant to the initial indentation of microneedles). Furthermore, the findings from these models do require experimental validation, which is the main limitation of this study. Measuring the individual RF on MNs within an array is exceptionally challenging due to their size, but needs to be considered in future work. Whilst the specific findings of this study have not been validated, the material model used was previously validated for use with MNs (Groves et al. 2012).

A further limitation of this work is the omission of skin puncture in the analysis. However, unlike indentation, the mechanics of skin fracture at the size scale of microneedles is poorly understood, largely due to the great difficulty in isolating appropriate skin samples and extracting robust measurements of the fracture properties of the individual sub-layers (e.g., stratum corneum, viable epidermis, dermis).

Since the goal of this work was to clarify the relationship between MN spacing, skin strain and needle RF, the analysis was therefore limited to indentation, where skin layer thickness and validated material models are sufficient to gain robust insights.

Furthermore, while studying the progressive failure of the skin as the needle inserts is undoubtedly important, obtaining consistent puncturing of the skin is a major challenge for microneedle design and a worthwhile objective in of itself. This work shed light on the mechanics of microneedle insertion as it approaches the puncture event, demonstrating how MN spacing and other parameters (e.g., skin layer thicknesses) affect needle RF and the build-up of skin strain under each needle. While only a relatively small MN displacement could be studied (0.25 mm), due to the difficulty in modelling some challenging

parameter sets, the information produced here is useful towards understanding how to equalize the mechanical response across all needles of the array during the indentation phase and, therefore, the puncture event when the skin eventually fails.

The modelling techniques presented here offer a valuable tool for microneedle array and applicator design, allowing for an investigation that is otherwise difficult to perform *in vitro* or *in vivo*, given the large number of variables and the size scale involved. Future work aims to expand these techniques to include MN penetration, with supporting validation made through practical experimentation with MNs and Micro-CT imaging.

## 4. Conclusions

The aim of this study was to determine the relationship between MN spacing, needle RF and skin strain, and to provide information for optimisation of MN arrays. We demonstrate through both a two-needle spacing sensitivity analysis and a nine-needle spacing analysis that spacings smaller than approximately 2–3 mm will result in differing needle forces across the array and hence may require more sophisticated design to ensure uniform penetration. The study also confirmed the importance of skin pre-stretch, needle geometry, and the properties and thickness of the epidermis, but it was found that the thickness and properties of the dermis and hypodermis had little influence, suggesting that the precise site and the thickness of subdermal tissue may be less important.

## Acknowledgements

The authors would like to acknowledge Mr Paul Aaron for his contributions towards the initial development of the MN indentation models.


## Disclosure Statement

No potential conflict of interest was reported by the author(s).

## Funding

This work is part of a wider collaborative project funded by the Bill & Melinda Gates Foundation (INV-010030, INV-009575). The authors received the support of the funders and all members of the project consortium.

## ORCID

Matthew R. Potts  <http://orcid.org/0000-0003-4197-906X>  
Sam L. Evans  <http://orcid.org/0000-0003-3664-2569>



Rhys Pullin  <http://orcid.org/0000-0002-2853-6099>  
 Sion A. Coulman  <http://orcid.org/0000-0002-1277-7584>  
 James C. Birchall  <http://orcid.org/0000-0001-8521-6924>  
 Hayley Wyatt  <http://orcid.org/0000-0001-6893-1977>

## References

- Donnelly RF, Garland MJ, Morrow DI, Migalska K, Singh TR, Majithiya R, Woolfson AD. 2010. Optical coherence tomography is a valuable tool in the study of the effects of microneedle geometry on skin penetration characteristics and in-skin dissolution. *J Control Release*. 147(3): 333–341.
- Evans SL, Holt CA. 2009. Measuring the mechanical properties of human skin in vivo using digital image correlation and finite element modelling. *J Strain Anal Eng Des*. 44(5):337–345.
- Flynn C, Taberner A, Nielsen P. 2011. Modeling the mechanical response of in vivo human skin under a rich set of deformations. *Ann Biomed Eng*. 39(7):1935–1946.
- Gambichler T, Matip R, Moussa G, Altmeyer P, Hoffmann K. 2006. In vivo data of epidermal thickness evaluated by optical coherence tomography: effects of age, gender, skin type, and anatomic site. *J Dermatol Sci*. 44(3): 145–152.
- Groves RB, Coulman SA, Birchall JC, Evans SL. 2012. Quantifying the mechanical properties of human skin to optimise future microneedle device design. *Comput Methods Biomech Biomed Engin*. 15(1):73–82.
- Guillot AJ, Cordeiro AS, Donnelly RF, Montesinos MC, Garrigues TM, Melero A. 2020. Microneedle-Based Delivery: An Overview of Current Applications and Trends. *Pharmaceutics*. 12(6):569.
- Joodaki H, Panzer MB. 2018. Skin mechanical properties and modelling: A review. *Proc Inst Mech Eng H*. 232(4): 323–343.
- Kim J, Park S, Nam G, Choi Y, Woo S, Yoon SH. 2018. Bioinspired microneedle insertion for deep and precise skin penetration with low force: why the application of mechanophysical stimuli should be considered. *J Mech Behav Biomed Mater*. 78:480–490.
- Kochhar JS, Quek TC, Soon WJ, Choi J, Zou S, Kang L. 2013. Effect of microneedle geometry and supporting substrate on microneedle array penetration into skin. *J Pharm Sci*. 102(11):4100–4108.
- Larraneta E, Lutton RE, Woolfson AD, Donnelly RF. Microneedle arrays as transdermal and intradermal drug delivery systems: Materials science, manufacture and commercial development. *Mater Sci Eng*. 104:1–32.
- Maas SA, Ellis BJ, Ateshian GA, Weiss JA. 2012. FEBio: finite elements for biomechanics. *J Biomech Eng*. 134(1): 011005.
- Moore TL, Lunt M, McManus B, Anderson ME, Herrick AL. 2003. Seventeen-point dermal ultrasound scoring system—a reliable measure of skin thickness in patients with systemic sclerosis. *Rheumatology (Oxford)*. 42(12): 1559–1563.
- Oh JH, Park HH, Do KY, Han M, Hyun DH, Kim CG, Kim CH, Lee SS, Hwang SJ, Shin SC, et al. 2008. Influence of the delivery systems using a microneedle array on the permeation of a hydrophilic molecule, calcitonin. *Eur J Pharm Biopharm*. 69(3):1040–1045.
- Olatunji O, Das DB, Garland MJ, Belaid L, Donnelly RF. 2013. Influence of array interspacing on the force required for successful microneedle skin penetration: theoretical and practical approaches. *J Pharm Sci*. 102(4): 1209–1221.
- Prausnitz MR. 2004. Microneedles for transdermal drug delivery. *Adv Drug Deliv Rev*. 56(5):581–587.
- Römgens AM, Bader DL, Bouwstra JA, Baaijens F, Oomens C. 2014. Monitoring the penetration process of single microneedles with varying tip diameters. *J Mech Behav Biomed Mater*. 40:397–405.
- Sabri AH, Cater Z, Ogilvie J, Scurr DJ, Marlow M, Segal J. 2020. Characterisation of mechanical insertion of commercial microneedles. *J Drug Deliv Sci Technol*. 58: 101766.
- Shu W, Heimark H, Bertollo N, Tobin DJ, O’Cearbhaill ED, Annaidh AN. 2021. Insights into the mechanics of solid conical microneedle array insertion into skin using the finite element method. *Acta Biomater*. 135:403–413.
- Verbaan FJ, Bal SM, van den Berg DJ, Dijkman JA, van Hecke M, Verpoorten H, van den Berg A, Luttge R, Bouwstra JA. 2008. Improved piercing of microneedle arrays in dermatomed human skin by an impact insertion method. *J Control Release*. 128(1):80–88.